

Lightweight and Flexible Deep Equilibrium Learning for CSI Feedback in FDD Massive MIMO

Yifan Ma*, Wentao Yu*, Xianghao Yu[†], Jun Zhang*, Shenghui Song*, and Khaled B. Letaief*

*Dept. of ECE, The Hong Kong University of Science and Technology, Hong Kong

[†]Dept. of EE, City University of Hong Kong, Hong Kong

Email: *{ymabj, wyuaq, eejzhang, eeshsong, eekhaled}@ust.hk, [†]alex.yu@cityu.edu.hk

Abstract—In frequency-division duplexing (FDD) massive multiple-input multiple-output (MIMO) systems, downlink channel state information (CSI) needs to be sent back to the base station (BS) by the users, which causes prohibitive feedback overhead. In this paper, we propose a lightweight and flexible deep learning-based CSI feedback approach by capitalizing on deep equilibrium models. Different from existing deep learning-based methods that stack multiple explicit layers, we propose an implicit equilibrium block to mimic the behavior of an infinite-depth neural network. In particular, the implicit equilibrium block is defined by a fixed-point iteration and the trainable parameters in different iterations are shared, which results in a lightweight model. Furthermore, the number of forward iterations can be adjusted according to users' computation capability, enabling a flexible accuracy-efficiency trade-off. Simulation results will show that the proposed design obtains a comparable performance as the benchmarks but with much-reduced complexity and permits an accuracy-efficiency trade-off at runtime.

I. INTRODUCTION

Massive multiple-input multiple-output (MIMO) systems are regarded as a key enabler for 5G and beyond wireless communication systems [1] where frequency-division duplexing (FDD) is considered a compelling operation mode. In FDD massive MIMO systems, users need to feed the downlink channel state information (CSI) back to the base station (BS) to facilitate beamforming. However, the dimension of the CSI increases significantly as the number of antennas at the BS gets larger, which causes prohibitive feedback overhead. Conventional compressive sensing (CS)-based methods were widely applied for CSI compression and recovery [2], but they suffered from noteworthy limitations, such as the impractical assumption of channel sparsity, the limited ability to exploit the channel structures, and the high computational cost of the iterative operations [3].

Thanks to the the universal approximation capability of neural networks, the deep learning-based auto-encoder and decoder structures have been leveraged to effectively compress and reconstruct the downlink CSI. The exploratory work [3] proposed a convolutional neural network (CNN)-based CsiNet which outperforms the CS-based algorithms especially with low compression ratios. Several subsequent studies, including ConvCsiNet [4] and TransNet [5], aimed to further improve the feedback accuracy using deeper CNNs and attention mechanism, respectively. However, the performance improvement is at the cost of computational complexity. For example, the number of floating point operations (FLOPs) of ConvCsiNet is almost one hundred times that of CsiNet. This puts prohibitive

burdens on memory and computational resources, making the deployment of these deep learning-based designs challenging in practice.

To reduce the huge execution cost, various lightweight schemes were proposed. Efficient neural network architectures were designed by replacing redundant neural network layers with simplified compositions. For example, the vanilla convolutional layers were replaced by shuffle layers in [4] to achieve a comparable accuracy with 1/3 FLOPs of ConvCsiNet. However, existing models can not fit the dynamic communication environment. In practice, the computational budget varies (e.g., numerous background applications can reduce the available computational resource) and the energy budget differs (e.g., a mobile phone may be in the power-saving mode). As such, different models need to be pre-trained, stored, and allocated to different devices/conditions according to the dynamic resource budget, leading to large memory and time cost. Hence, it is of great value to develop new models that provide a flexible trade-off between accuracy and efficiency.

In this paper, we propose a lightweight and flexible CSI feedback approach for FDD massive MIMO systems, allowing an accuracy-efficiency trade-off at runtime. Instead of stacking multiple well-designed *explicit* layers, i.e., the output is computed by explicitly cascading a series of nonlinear mappings, we develop a learning model composed of *implicit* equilibrium blocks. Specifically, the equilibrium block specifies the input-output relationship by a fixed-point equation. The forward propagation is a fixed-point finding process, which is separated from the backward neural network training, keeping a constant memory consumption of the backpropagation [6]. Besides, the trainable parameters in different iterations are shared, which results in a lightweight model. To meet the dynamically changing computation capability in practice, the number of implicit iterations at the users and the BS can be adjusted according to latency and computational budget during the inference stage. Extensive simulation results show that the proposed method outperforms the conventional CsiNet [3] and has a comparable or even better performance than the existing approaches [4] with greatly reduced complexity.

II. SYSTEM MODEL AND PROBLEM FORMULATION

This work considers a single-cell FDD massive MIMO system where the BS is equipped with N_t transmit antennas and the user is equipped with a single receive antenna. For ease of illustration, a single user case is considered while

the proposed scheme can be easily generalized to the multi-user scenario. An orthogonal frequency division multiplexing (OFDM) system with N_c subcarriers is considered. The received signal on the n -th subcarrier is expressed as

$$y_n = \mathbf{h}_n^H \mathbf{v}_n x_n + z_n, \quad (1)$$

where $\mathbf{h}_n \in \mathbb{C}^{N_t \times 1}$, $\mathbf{v}_n \in \mathbb{C}^{N_t \times 1}$, $x_n \in \mathbb{C}$, and $z_n \in \mathbb{C}$ denote the downlink channel vector, the downlink beamforming vector, the transmit symbol, and the additive noise of the n -th subcarrier, respectively. The CSI matrix over all subcarriers is thus denoted by $\mathbf{H} = [\mathbf{h}_1, \dots, \mathbf{h}_{N_c}]^H \in \mathbb{C}^{N_c \times N_t}$. The downlink beamforming design requires the BS to know the downlink CSI. In this paper, we assume that the downlink channel is perfectly known at the user side via pilot-based training and focus on the efficient feedback design [3]–[5].

Considering that the channel matrix \mathbf{H} contains $2N_c N_t$ real elements and the feedback overhead is prohibitive for FDD massive MIMO system, we first sparsify \mathbf{H} in the angular-delay domain using a 2D discrete Fourier transform (2D-DFT) [3] as follows

$$\mathbf{H}' = \mathbf{F}_d \mathbf{H} \mathbf{F}_a, \quad (2)$$

where $\mathbf{F}_d \in \mathbb{C}^{N_c \times N_c}$ and $\mathbf{F}_a \in \mathbb{C}^{N_t \times N_t}$ are two DFT matrices. Only the first N_a rows of \mathbf{H}' contain significant values and other elements are close to zero because the time delays between multipath arrivals are within a limited period [3]. Therefore, we take the first N_a rows of \mathbf{H}' ($N_a < N_c$) and define a new matrix $\mathbf{H}'' \in \mathbb{C}^{N_a \times N_t}$. By doing this, we can compress \mathbf{H}'' instead of \mathbf{H} with only $2N_a N_t$ entries and imperceptible information loss.

In this work, a deep learning-based method is proposed for CSI compression and recovery. The encoding process at the user side is given by

$$\mathbf{s} = \mathcal{E}_{\theta_e}(\mathbf{H}''), \quad (3)$$

which further compresses the channel matrix into an $M \times 1$ codeword \mathbf{s} . The parameterized mapping $\mathcal{E}_{\theta_e}(\cdot)$ denotes the compression procedure and θ_e is the trainable parameters in the encoder. The compression ratio is defined as $\gamma = M/2N_a N_t$. We use the same setting as [3]–[5] and assume \mathbf{s} is sent back to the BS via error-free transmission. After receiving the codeword, the BS reconstructs the channel matrix through a decoder, expressed as

$$\hat{\mathbf{H}}'' = \mathcal{D}_{\theta_d}(\mathbf{s}), \quad (4)$$

where $\mathcal{D}_{\theta_d}(\cdot)$ denotes the recovery procedure and θ_d represents the trainable parameters at the decoder. The objective is to minimize the mean-squared-error (MSE) between the recovered channel and the true channel, given by

$$\min_{\theta_e, \theta_d} \mathbb{E} \{ \|\mathbf{H}'' - \mathcal{D}_{\theta_d}(\mathcal{E}_{\theta_e}(\mathbf{H}''))\|_2^2 \}. \quad (5)$$

The mapping $\mathcal{E}_{\theta_e}(\cdot)$ and $\mathcal{D}_{\theta_d}(\cdot)$ can be instantiated as an auto-encoder and a decoder, and jointly trained via end-to-end learning [3]–[5]. However, most of the existing works improve the reconstruction accuracy at the cost of high neural network complexity, which is not affordable for mobile devices due to limited resources. Moreover, the existing feedback schemes

lack an effective mechanism to achieve the performance-complexity trade-off during execution. In practice, different devices have different runtime for a neural network [7]. Given the same latency budget, high-end devices can achieve better performance by running complicated models, while low-end ones have to sacrifice accuracy to meet the response time constraint. Even for the same device, the resource availability varies under different situations. Therefore, it is of vital importance to design a lightweight and flexible method for CSI feedback.

III. PROPOSED CSI FEEDBACK SCHEME WITH DEEP EQUILIBRIUM LEARNING

In this section, we first present the overall diagram of the proposed deep equilibrium learning-based CSI feedback scheme and the delicate design of the encoding and decoding blocks. As two key advantages, we then present the lightweight and flexible inference procedure and a low-complexity training procedure.

A. Overall Structure

The widely adopted explicit deep neural network model can be written as

$$\mathbf{y}_{\text{out}}^{[i+1]} = f_{\theta}^{[i+1]}(\mathbf{y}_{\text{out}}^{[i]}; \mathbf{x}_{\text{in}}), \quad i = 0, 1, \dots, L-1, \quad (6)$$

where $\mathbf{y}_{\text{out}}^{[i]}$ is the output of the i -th layer, $f_{\theta}^{[i]}$ represents the i -th layer's parameterized function, \mathbf{x}_{in} denotes the input, and L is the number of layers. Recent findings in [8] showed that employing the same transformation function in each layer still leads to competitive results. The shared-weight neural network is correspondingly expressed as

$$\mathbf{y}_{\text{out}}^{[i+1]} = f_{\theta}(\mathbf{y}_{\text{out}}^{[i]}; \mathbf{x}_{\text{in}}), \quad i = 0, 1, \dots, L-1, \quad (7)$$

and thus the number of trainable parameters is greatly reduced. Note that stacking an infinite number of weight-sharing layers corresponds to finding the fixed-point solution of the equation [6], [9]

$$\mathbf{y}_{\text{out}}^* = f_{\theta}(\mathbf{y}_{\text{out}}^*; \mathbf{x}_{\text{in}}). \quad (8)$$

The implicit equilibrium model allows us to directly find the equilibrium point $\mathbf{y}_{\text{out}}^*$ with an off-the-shelf solver or iteratively executing $f_{\theta}(\cdot)$. Besides, according to the implicit function theorem, the backward propagation is independent of the forward fixed-point finding process, making the trainable weight update equivalent to one single layer.

With the same trainable parameters in each iteration, the output and all hidden units of conventional deep equilibrium learning should have the same dimensions. Nevertheless, for the CSI compression and recovery task, the input channel matrix needs to be downsampled and upsampled to guarantee $M \ll 2N_a N_t$. Hence, it is not feasible if we only apply equilibrium blocks for the mappings in (3) and (4). Furthermore, the computation capability of mobile users is generally limited, which requires a simple yet effective encoder to be deployed at the user side. Based on these two aspects, we incorporate the implicit equilibrium block with traditional explicit neural network design. The overall diagram is shown in Fig. 1 and the operations at the test stage are summarized in **Algorithm 1**.

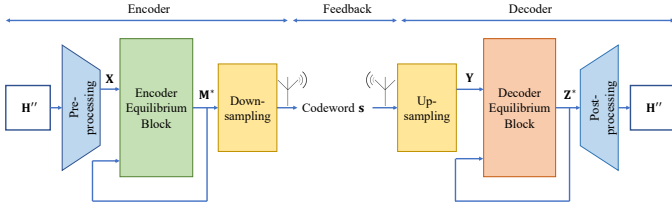


Fig. 1. Diagram of the proposed deep equilibrium learning-based CSI feedback scheme.

Algorithm 1 Inference Stage of the Proposed CSI Feedback Scheme with Deep Equilibrium Learning

- 1: **Input:** Truncated channel matrix in angular-delay domain \mathbf{H}'' . Well-trained encoding blocks f_{pre} , f_{eim} , and f_{down} . The FLOPs number of encoding blocks F_{pre} , F_{eim} , and F_{down} . Well-trained decoding blocks f_{up} , f_{dim} , and f_{post} . The FLOPs number of decoding blocks F_{up} , F_{dim} , and F_{post} . Computational budget R_e and R_d at the user side and the BS side, respectively.
- 2: **Output:** Reconstructed channel matrix $\hat{\mathbf{H}}''$
- 3: **Encoder:**
- 4: $\mathbf{X} \leftarrow f_{\text{pre}}(\mathbf{H}'')$
- 5: $\mathbf{M}^{[0]} \leftarrow \mathbf{X}$
- 6: $T_e \leftarrow \lfloor \frac{R_e - F_{\text{pre}} - F_{\text{down}}}{F_{\text{eim}}} \rfloor$
- 7: **for** $t \leftarrow 1$ to T_e **do**
- 8: $\mathbf{M}^{[t]} \leftarrow f_{\text{eim}}(\mathbf{M}^{[t-1]}, \mathbf{X})$
- 9: **end for**
- 10: $\mathbf{s} \leftarrow f_{\text{down}}(\mathbf{M}^{[T_e]})$
- 11: **Decoder:**
- 12: $\mathbf{Y} \leftarrow f_{\text{up}}(\mathbf{s})$
- 13: $\mathbf{Z}^{[0]} \leftarrow \mathbf{Y}$
- 14: $T_d \leftarrow \lfloor \frac{R_d - F_{\text{up}} - F_{\text{post}}}{F_{\text{dim}}} \rfloor$
- 15: **for** $t \leftarrow 1$ to T_d **do**
- 16: $\mathbf{Z}^{[t]} \leftarrow f_{\text{dim}}(\mathbf{Z}^{[t-1]}, \mathbf{Y})$
- 17: **end for**
- 18: $\hat{\mathbf{H}}'' \leftarrow f_{\text{post}}(\mathbf{Z}^{[T_d]})$

Mathematically, the encoding process is expressed as

$$\begin{aligned} \mathbf{X} &= f_{\text{pre}}(\mathbf{H}''), \\ \mathbf{M}^{[t]} &= f_{\text{eim}}(\mathbf{M}^{[t-1]}, \mathbf{X}), \quad t = 1, \dots, T_e, \\ \mathbf{s} &= f_{\text{down}}(\mathbf{M}^*). \end{aligned} \quad (9)$$

$f_{\text{pre}}(\cdot)$ is the preprocessing block to form the input injection \mathbf{X} . The input injection is pivotal to equilibrium models. Since the fixed-point \mathbf{M}^* does not depend on any initial value of $\mathbf{M}^{[0]}$, preprocessing \mathbf{H}'' and injecting \mathbf{X} properly ensures the dependency between the fixed-point and the model input. $f_{\text{eim}}(\cdot, \cdot)$ and T_e denote the encoder-side implicit equilibrium block and the number of iterations, respectively. Note that the hyperparameter T_e can be adjusted flexibly during runtime according to the resource budget. Therefore, it provides us with a flexible CSI feedback approach applicable in different scenarios without additional training or model downloading costs. Details of flexible implementation will be discussed in Section III-C. The output of the implicit model \mathbf{M}^* is then fed into the downsampling block $f_{\text{down}}(\cdot)$ which reduces the

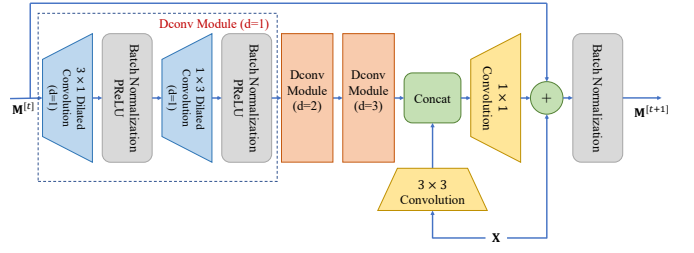


Fig. 2. The implicit equilibrium block at the encoder.

output into M dimensions. The codeword \mathbf{s} is then transmitted back to the BS.

At the BS side, the decoding process is given by

$$\begin{aligned} \mathbf{Y} &= f_{\text{up}}(\mathbf{s}), \\ \mathbf{Z}^{[t]} &= f_{\text{dim}}(\mathbf{Z}^{[t-1]}, \mathbf{Y}), \quad t = 1, \dots, T_d, \\ \hat{\mathbf{H}}'' &= f_{\text{post}}(\mathbf{Z}^*), \end{aligned} \quad (10)$$

where $f_{\text{up}}(\cdot)$ represents the upsampling block, \mathbf{Y} is the input injection of the decoder-side implicit equilibrium block $f_{\text{dim}}(\cdot, \cdot)$, $\mathbf{Z}^{[0]}$ is the initial value, T_d denotes the maximum number of iterations, and $f_{\text{post}}(\cdot)$ is the post-processing block. The detailed structure of two equilibrium blocks will be discussed in the following subsection.

B. Design of Encoding and Decoding Blocks

1) *Encoder:* The input to the encoder is the real and the imaginary parts of \mathbf{H}'' , forming a $2 \times N_a \times N_t$ dimensional tensor. The preprocessing module of the encoder, i.e., $f_{\text{pre}}(\cdot)$, is constructed by 5×5 convolutional kernels followed by batch normalization and parametric rectified linear unit (PReLU) activation functions. The PReLU function with a learnable parameter α is given by

$$\text{PReLU}(x) = \begin{cases} x, & x \geq 0 \\ \alpha x, & x < 0. \end{cases} \quad (11)$$

This module effectively extracts the information from the input CSI matrix and fuses the features from both the real and the imaginary parts at an affordable cost. The output of the preprocessing module is treated as the input injection to the implicit equilibrium block. The major component of the equilibrium module is the transformation function $f_{\text{eim}}(\cdot, \cdot)$. Inspired by the fact that the CNN-based autoencoder can efficiently extract the spatially local correlation in the CSI matrices [3], we develop the $f_{\text{eim}}(\cdot, \cdot)$ by using a CNN-based structure, as shown in Fig. 3. To improve the CSI reconstruction accuracy without increasing computational cost, dilated convolutions [10] are adopted. The 2D-dilated convolutional operation without bias is written as

$$(\mathbf{I} \otimes \mathbf{K})[i, j] = \sum_m \sum_n \mathbf{I}[i + d \times m, j + d \times n] \cdot \mathbf{K}[m, n], \quad (12)$$

where \otimes , d , \mathbf{I} , and \mathbf{K} denote the dilated convolution operator, dilated rate, input tensor, and convolutional kernel, respectively. m and n are the indices of convolutional kernel \mathbf{K} . When $d = 1$, the dilated convolution degenerates into the standard convolution. When $d > 1$, the dilated convolution

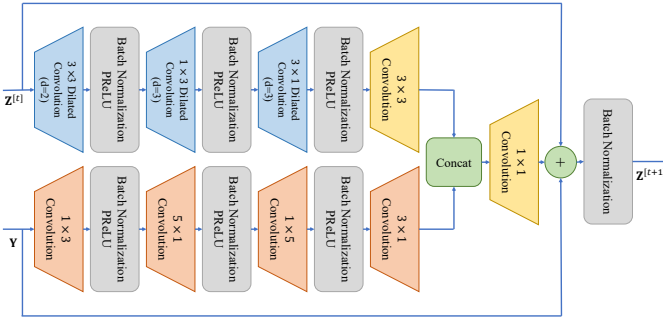


Fig. 3. The implicit equilibrium block at the decoder.

operation provides a larger receptive field compared to the standard convolution with the same kernel size. To promote good performance and diminish information loss, three consecutive dilated convolution modules are employed. In each dilated convolution module, 3×1 and 1×3 kernels are applied to better extract the vertical and horizontal information. Besides, inspired by the residual network [11], the identity shortcut connections of latent space variable $\mathbf{M}^{[t]}$ and input \mathbf{X} are introduced. After the equilibrium module, the last downsampling block in the encoder is implemented by one fully-connected layer.

2) *Decoder*: After receiving the codeword \mathbf{s} , a fully-connected layer is adopted as $f_{\text{up}}(\cdot)$ to recover the dimension of CSI matrix, forming the input injection \mathbf{Y} to the implicit equilibrium block. Similar to $f_{\text{eim}}(\cdot, \cdot)$, we design the decoder-side implicit equilibrium block $f_{\text{dim}}(\cdot, \cdot)$ with two parallel branches and identity shortcuts. The powerful computation capability at the BS can support more complicated operations than the users and thus improve the overall reconstruction performance. Instead of using one standard convolution for input injection, we adopt four consecutive convolutions at the decoder. In addition, the number of feature maps is expanded from 2 to 80. The other settings are identical with the encoder. The sigmoid mapping is adopted as the post-processing function $f_{\text{post}}(\cdot)$.

C. Flexibility

The number of FLOPs is used to measure the time complexity of a learning model. To show the flexible execution of our proposed method, we first evaluate the number of FLOPs of different deep learning components. The number of FLOPs of a fully-connected layer with bias is given by

$$F_{\text{fc}} = 2I_{\text{in}}I_{\text{out}}, \quad (13)$$

where I_{in} and I_{out} denote the input dimension and output dimension, respectively. The number of FLOPs of a convolutional layer with bias is expressed as

$$F_{\text{conv}} = 2C_{\text{in}}K^2HWC_{\text{out}}, \quad (14)$$

where K is the kernel size. H and W are the height and the width of the output feature map, respectively. C_{in} and C_{out} denote the numbers of input and output channels, respectively. According to (13) and (14), the number of FLOPs of each

proposed block can be computed. The total number of FLOPs of the proposed encoder F_e and decoder F_d is then given by

$$\begin{aligned} F_e &= F_{\text{pre}} + T_e \times F_{\text{eim}} + F_{\text{down}}, \\ F_d &= F_{\text{up}} + T_d \times F_{\text{dim}} + F_{\text{post}}, \end{aligned} \quad (15)$$

where F_i denotes the number of FLOPs of function f_i , for $i \in \{\text{pre}, \text{eim}, \text{down}, \text{up}, \text{dim}, \text{post}\}$.

Due to the dynamic communication environment, the available computation capability of devices varies from time to time. Given the computational budget R_e and R_d at the users and the BS, respectively, the number of FLOPs of the implemented encoder and decoder should not exceed the budget, i.e., $F_e \leq R_e$ and $F_d \leq R_d$. However, the F_e and F_d of conventional deep learning-based approaches are fixed once trained. Therefore, they lack a performance-efficiency trade-off at runtime and models with different complexity need to be trained, benchmarked, and deployed individually. Once the environment changes, i.e., R_e and/or R_d changes, one needs to switch to a larger or smaller model by downloading pre-trained weights, which consumes large memory and time cost. In contrast, in our proposed method, the number of iterations of encoding and decoding equilibrium blocks can be adjusted according to the resource budget, i.e.,

$$\begin{aligned} T_e &= \lfloor \frac{R_e - F_{\text{pre}} - F_{\text{down}}}{F_{\text{eim}}} \rfloor, \\ T_d &= \lfloor \frac{R_d - F_{\text{up}} - F_{\text{post}}}{F_{\text{dim}}} \rfloor. \end{aligned} \quad (16)$$

This enables a flexible trade-off between accuracy and complexity. When the resource budget varies, the proposed approach can adaptively select an appropriate iteration number and achieving an online accuracy-efficiency trade-off without re-training or downloading data.

D. Training Strategies

Since the encoding and decoding blocks share similar structures, we take the encoder side as an example for the ease of illustration. According to [6], [12], we can directly backpropagate the implicit equilibrium block using the Jacobian of f_{eim} at \mathbf{M}^* , i.e.,

$$\begin{aligned} \frac{\partial \ell}{\partial \theta} &= \frac{\partial \ell}{\partial \mathbf{M}^*} (\mathbf{I} - \mathbf{J}_{f_{\text{eim}}} |_{\mathbf{M}^*})^{-1} \frac{\partial f_{\text{eim}}(\mathbf{M}^*, \mathbf{X})}{\partial \theta}, \\ \frac{\partial \ell}{\partial \mathbf{X}} &= \frac{\partial \ell}{\partial \mathbf{M}^*} (\mathbf{I} - \mathbf{J}_{f_{\text{eim}}} |_{\mathbf{M}^*})^{-1} \frac{\partial f_{\text{eim}}(\mathbf{M}^*, \mathbf{X})}{\partial \mathbf{X}}, \end{aligned} \quad (17)$$

where ℓ denotes the training loss, θ denotes the trainable parameters, \mathbf{I} is the identity matrix, and $\mathbf{J}_{f_{\text{eim}}} |_{\mathbf{M}^*}$ represents the Jacobian of f_{eim} at \mathbf{M}^* . Since the computation of the inverse Jacobian is complicated, we further adopt the approximated gradient descent direction in [13]

$$\begin{aligned} \hat{\frac{\partial \ell}{\partial \theta}} &= \frac{\partial \ell}{\partial \mathbf{M}^*} \frac{\partial f_{\text{eim}}(\mathbf{M}^*, \mathbf{X})}{\partial \theta}, \\ \hat{\frac{\partial \ell}{\partial \mathbf{X}}} &= \frac{\partial \ell}{\partial \mathbf{M}^*} \frac{\partial f_{\text{eim}}(\mathbf{M}^*, \mathbf{X})}{\partial \mathbf{X}}. \end{aligned} \quad (18)$$

It is proved in [13] that (18) is a descent direction of ℓ , even for approximate fixed-points. By adopting (18), we separate the forward fixed-point finding procedures from the

backward neural network training. The backpropagation is thus based on differentiating through one layer at the fixed-point, i.e., $\frac{\partial f_{\text{eim}}(\mathbf{M}^*, \mathbf{X})}{\partial \theta}$ and $\frac{\partial f_{\text{eim}}(\mathbf{M}^*, \mathbf{X})}{\partial \mathbf{X}}$. No intermediate values in the equilibrium block are required and the training memory consumption is constant, which is equivalent to training a one-layer neural network.

IV. SIMULATION RESULTS

In this section, we demonstrate the performance of the proposed lightweight and flexible CSI feedback approach for FDD massive MIMO systems.

A. Simulation Setup

1) *Data Generation*: Following the experimental settings in [3], an indoor picocellular system operating at the 5.3 GHz band is considered. The channel matrices are generated according to the COST 2100 models [14]. The BS is equipped with a uniform linear array with $N_t = 32$. The number of subcarriers is set as 1024. The original $2 \times 1024 \times 32$ CSI matrix is transformed into the angular-delay domain and truncated to the first 32 rows, forming the $2 \times 32 \times 32$ matrix \mathbf{H}'' .

2) *Training Settings*: The training, validation, and test datasets contain 100,000, 30,000, and 20,000 samples, respectively. The Adam optimizer is used for trainable weight updates. Kaiming initialization is used for each convolution operation and fully-connected layer. The numbers of epochs is 1000 and batch size is set to 200. During training, T_e and T_d are set to 10 and 5, respectively. The training loss is the MSE between the recovered CSI and the true CSI. The learning rate varies between $\eta_{\min} = 5 \times 10^{-5}$ and $\eta_{\max} = 0.001$, and the process can be expressed as

$$\eta_t = \eta_{\min} + \frac{1}{2} (\eta_{\max} - \eta_{\min}) \left(1 + \cos \left(\frac{t}{T} \pi \right) \right), \quad (19)$$

where η_t is the learning rate of the t -th epoch and T denotes total number of epochs.

3) *Evaluation Metric*: The normalized mean squared error (NMSE) between the recovered channel and the true channel is used to evaluate the performance, which is given by

$$\text{NMSE} = \mathbb{E} \left\{ \frac{\|\mathbf{H}'' - \hat{\mathbf{H}}''\|_2^2}{\|\mathbf{H}''\|_2^2} \right\}. \quad (20)$$

In addition, the number of FLOPs is used to measure the time complexity of the learning model, and the number of trainable parameters is adopted as a metric to measure the space complexity [4]. All the simulations are done using the existing deep learning platform PyTorch. The number of FLOPs and trainable parameters are calculated using the thop package [15] for PyTorch.

B. Performance Comparison

To illustrate the effectiveness of the proposed CSI feedback design, we adopt three benchmarks for comparison:

- **CsiNet** [3]: An exploratory work that enjoys low time and space complexity.
- **ConvCsiNet** [4]: A complicated CNN-based method that achieves good performance but induces heavy computational costs.

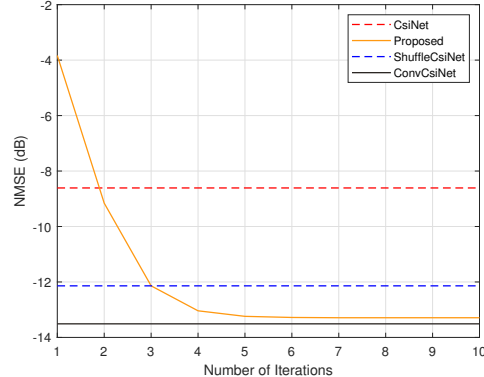


Fig. 4. NMSE achieved by different methods versus T_e when $\gamma = 1/16$ and $T_d = 5$.

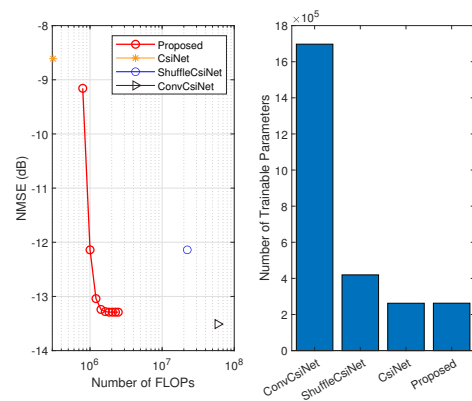


Fig. 5. Performance and complexity of different methods when $\gamma = 1/16$. (Left) NMSE achieved by different methods versus the number of FLOPs at the encoder side. (Right) The number of trainable parameters of different methods at the encoder side.

- **ShuffleCsiNet** [4]: An efficient neural network architecture is adopted, but the complexity is still high for users with extremely limited computational power.

Fig. 4 plots the NMSE achieved by the proposed deep equilibrium learning-based scheme and other baselines versus the number of iterations when $\gamma = 1/16$. Since the other baselines use explicit neural networks and the outputs are acquired through one forward propagation, they do not have the concept of iterations. It can be observed from Fig. 4 that running the proposed method with just 2 iterations outperforms CsiNet and 3 iterations outperforms ShuffleCsiNet, showing the superiority of the proposed scheme in terms of efficiency. Moreover, it is demonstrated that the proposed CSI feedback scheme converges with 7 iterations and achieves a comparable performance as ConvCsiNet.

In Fig. 5, we demonstrate the accuracy-efficiency trade-offs of different methods. In the left sub-figure, the NMSE achieved by different methods versus the number of FLOPs at the encoder side is demonstrated. It is shown that although CsiNet only requires a small number of FLOPs and induces low time complexity, the performance is not satisfactory. On the other hand, the ConvCsiNet method achieves around 5

TABLE I
PERFORMANCE AND ENCODER FLOPS FOR DIFFERENT COMPRESSION
RATIOS WHEN $T_e = 10$ AND $T_d = 5$

Compression Ratio γ	Method	NMSE (dB)	FLOPs (M)
1/4	ConvCsiNet	-15.13	60.69
	ShuffleCsiNet	-17.36	24.11
	CsiNet	-17.36	1.09
	Proposed	-19.82	3.25
1/8	ConvCsiNet	-14.38	59.51
	ShuffleCsiNet	-14.59	22.93
	CsiNet	-13.47	0.57
	Proposed	-15.30	2.73
1/16	ConvCsiNet	-13.51	58.92
	ShuffleCsiNet	-12.14	22.34
	CsiNet	-8.65	0.31
	Proposed	-13.29	2.46
1/32	ConvCsiNet	-10.34	58.62
	ShuffleCsiNet	-9.41	22.05
	CsiNet	-6.24	0.18
	Proposed	-9.31	2.33

dB higher accuracy compared with CsiNet, but it requires more than 58 million FLOPs. Assume that the compression ratio is 1/16 and the CSI feedback and recovery period is 1 millisecond. The computational power required by the ConvCsiNet encoder is about 59 G floating point operations per second (FLOPS) [4]. Note that Kirin 970, one of the mid- and high-end mobile systems on chip (SoC), has a total peak computation capability of 244.8 G FLOPS [16]. If the ConvCsiNet is deployed in practice, around 1/4 of the mobile's computational power is used for CSI feedback, making other computationally-intensive tasks such as graphics rendering and voice recognition unable to work.

In the left sub-figure of Fig. 5, it is also demonstrated that the proposed deep equilibrium learning-based CSI feedback design can achieve an instant accuracy-efficiency trade-off by adjusting the encoder-side equilibrium block iteration number at runtime, while for other baselines, the learning model is fixed once trained. Besides, after convergence, the performance of the deep equilibrium learning-based approach is comparable with ConvCsiNet while the number of FLOPs is greatly reduced.

In the right sub-figure of Fig. 5, the numbers of trainable parameters of different methods at the user side are plotted. Thanks to the weight sharing in the equilibrium block, the number of trainable parameters is greatly reduced, leading to a lower space complexity of the proposed scheme. It is also demonstrated that the ConvCsiNet has the highest space complexity among all the benchmarks. For example, when $\gamma = 1/16$, the ConvCsiNet encoder network needs to store more than 1 million floating point data, occupying about 6 MB of storage space [4]. In contrast, the proposed scheme only requires less than 0.27 million float data and thus less than 1.62 MB storage space. This verifies the high efficiency of the proposed CSI feedback design.

Table I presents the FLOPs and NMSE versus the compression ratios γ . It is demonstrated that ConvCsiNet method achieves the best performance when γ is small but the performance degrades when the compression ratio is large. On the other hand, CsiNet and ShuffleCsiNet work well when γ is large but the NMSE is not satisfactory when γ is

small. It is also observed that the proposed method obtains a comparable performance as the baselines for all considered γ and outperforms all the baselines when $\gamma = 1/4$ and $\gamma = 1/8$ with a significantly reduced number of FLOPs.

V. CONCLUSIONS

In this paper, we developed a deep equilibrium learning-based model for CSI feedback in FDD massive MIMO systems. In contrast to existing explicit deep neural networks whose output is characterized by successive non-linear layers, we utilized a fixed-point equation to specify the input-output relationship. The proposed approach is lightweight and permits a flexible accuracy-efficiency trade-off at runtime. Extensive simulation results demonstrated that the proposed scheme significantly reduces the memory and computational costs without compromising the performance, when compared with existing methods.

REFERENCES

- [1] F. Boccardi, R. W. Heath, A. Lozano, T. L. Marzetta, and P. Popovski, "Five disruptive technology directions for 5G," *IEEE Commun. Mag.*, vol. 52, no. 2, pp. 74–80, Feb. 2014.
- [2] J.-C. Shen, J. Zhang, K.-C. Chen, and K. B. Letaief, "High-dimensional CSI acquisition in massive MIMO: Sparsity-inspired approaches," *IEEE Systems Journal*, vol. 11, no. 1, pp. 32–40, Mar. 2017.
- [3] C.-K. Wen, W.-T. Shih, and S. Jin, "Deep learning for massive MIMO CSI feedback," *IEEE Wireless Commun. Lett.*, vol. 7, no. 5, pp. 748–751, Oct. 2018.
- [4] Z. Cao, W.-T. Shih, J. Guo, C.-K. Wen, and S. Jin, "Lightweight convolutional neural networks for CSI feedback in massive MIMO," *IEEE Commun. Letters*, vol. 25, no. 8, pp. 2624–2628, Aug. 2021.
- [5] Y. Cui, A. Guo, and C. Song, "TransNet: Full attention network for CSI feedback in FDD massive MIMO system," *IEEE Wireless Commun. Lett.*, vol. 11, no. 5, pp. 903–907, May 2022.
- [6] S. Bai, J. Z. Kolter, and V. Koltun, "Deep equilibrium models," in *Proc. Advances Neural Inf. Process. Syst.*, vol. 32, Vancouver, Canada, Dec. 2019, pp. 690–701.
- [7] A. Ignatov, R. Timofte, W. Chou, K. Wang, M. Wu, T. Hartley, and L. Van Gool, "AI benchmark: Running deep neural networks on android smartphones," 2018. [Online]. Available: <https://arxiv.org/abs/1810.01109>
- [8] M. Dehghani, S. Gouws, O. Vinyals, J. Uszkoreit, and Ł. Kaiser, "Universal transformers," in *Proc. Int. Conf. Learn. Representations (ICLR)*, New Orleans, USA, May 2019, pp. 1–12.
- [9] W. Yu, Y. Shen, H. He, X. Yu, J. Zhang, and K. B. Letaief, "Hybrid far- and near-field channel estimation for THz ultra-massive MIMO via fixed point networks," in *Proc. IEEE Global Commun. Conf.*, Rio de Janeiro, Brazil, Dec. 2022, pp. 1–6.
- [10] S. Tang, J. Xia, L. Fan, X. Lei, W. Xu, and A. Nallanathan, "Dilated convolution based CSI feedback compression for massive MIMO systems," *IEEE Trans. Veh. Technol.*, vol. 71, no. 10, pp. 11 216–11 221, Oct. 2022.
- [11] K. He, X. Zhang, S. Ren, and J. Sun, "Deep residual learning for image recognition," in *Proc. IEEE Conf. Comput. Vision Pattern Recognit.*, Las Vegas, USA, June 2016, pp. 770–778.
- [12] S. Bai, V. Koltun, and J. Z. Kolter, "Multiscale deep equilibrium models," in *Proc. Advances Neural Inf. Process. Syst.*, vol. 33, Dec. 2020, pp. 5238–5250.
- [13] S. W. Fung, H. Heaton, Q. Li, D. McKenzie, S. Osher, and W. Yin, "JFB: Jacobian-free backpropagation for implicit networks," in *Proc. AAAI Conf. Artif. Intell.*, vol. 36, no. 6, Arlington, Virginia, USA, Feb. 2022, pp. 6648–6656.
- [14] L. Liu, C. Oestges, J. Poutanen, K. Haneda, P. Vainikainen, F. Quitin, F. Tufvesson, and P. D. Doncker, "The COST 2100 MIMO channel model," *IEEE Wireless Commun.*, vol. 19, no. 6, pp. 92–99, Dec. 2012.
- [15] GitHub, "Thop: Pytorch-OpCounter," <https://github.com/Lyken17/pytorch-OpCounter>.
- [16] S. Wang, A. Pathania, and T. Mitra, "Neural network inference on mobile SoCs," *IEEE Design & Test*, vol. 37, no. 5, pp. 50–57, Jan. 2020.